RESEARCH ARTICLE
SOLID EARTH: GEODESY AND GRAVITY

*Earth and Planetary Physics*
*7*: 487–498, 2023
doi: 10.26464/epp2023041

# Moho depth inversion in the Tibetan Plateau from high-precision gravity data

**HuiYou He[1,2], Jian Fang[1*], HePing Sun[1], DongMei Guo[1], ZhiXin Xue[1,2,3], and Jing Hou[1,3]**

[1]State Key Laboratory of Geodesy and Earth's Dynamics, Innovation Academy for Precision Measurement Science and Technology, Chinese Academy of Sciences, Wuhan 430077, China;

[2]Wuhan Gravitation and Solid Earth Tides National Observation and Research Station, Wuhan 430071, China;

[3]University of Chinese Academy of Sciences, Beijing 100049, China

**Key Points:**

- The 2159-order high-precision gravity field model (SGG-UGM-2) was combined with the CRUST1.0 model to eliminate the influence of extraneous factors to accurately obtain the high-precision Moho gravity anomaly of the Tibetan Plateau.
- Within the constraints of the diverse seismic profiles, the parameters essential for the Moho inversion — namely, average depth and interface density difference — were discerned with finesse and precision.
- The Bott iteration method was ingeniously devised to amplify the iteration efficiency and precision of the Parker–Oldenburg inversion method and the Moho depth in the Tibetan Plateau was expeditiously and effectively obtained with remarkable precision. The Moho in this area evinced the distinctive features of two depressions and two uplifts.

**Citation:** He, H. Y., Fang, J., Sun, H. P., Guo, D. M., Xue, Z. X., and Hou, J. (2023). Moho depth inversion in the Tibetan Plateau from high-precision gravity data. *Earth Planet. Phys.*, *7*(4), 487–498. http://doi.org/10.26464/epp2023041

**Abstract:** The Tibetan Plateau (TP) is the youngest orogenic belt resulting from a continental collision on the Earth. It is a natural laboratory for studying continental dynamics, such as continental convergence, plate subduction, and plateau uplift. Investigating the deep structure of the TP has always been a popular issue in geological research. The Moho is the boundary between the crust and the mantle and therefore plays a crucial role in the Earth's structure. Parameters such as depth and lateral variation, as well as the fine structure of the crust–mantle interface, reveal the lithospheric dynamics in the TP. Two methods are generally employed to study the Moho surface: seismic detection and gravity inversion. Seismic detection has the characteristic of high precision, but it is limited to a few cross-sectional lines and is quite costly. It is not suitable for and cannot be carried out over a large area of the TP. The Moho depth over a large area can be obtained through gravity inversion, but this method is affected by the nature of gravity data, and the accuracy of the inversion method is lower than that of seismic detection. In this work, a high-precision gravity field model was selected. The Parker–Oldenburg interface inversion method was used, within the constraints of seismic observations, and the Bott iteration method was introduced to enhance the inversion efficiency. The Moho depth in the TP was obtained with high precision, consistent with the seismic detection results. The research results showed that the shape of the Moho in the TP is complex and the variation range is large, reaching 60–80 km. In contrast with the adjacent area, a clear zone of sharp variation appears at the edge of the plateau. In the interior of the TP, the buried depth of the Moho is characterized by two depressions and two uplifts. To the south of the Yarlung Zangbo River, the Moho inclines to the north, and to the north, the Moho depresses downward, which was interpreted as the Indian plate subducting to the north below Tibet. The Moho depression on the north side of the Qiangtang block, reaching 72 km deep, may be a result of the southward subduction of the lithosphere. The Moho uplift of the Qiangtang block has the same strike as the Bangong–Nujiang suture zone, which may indicate that the area is compensated by a low-density and low-velocity mantle.

**Keywords:** gravity; Moho; Tibetan Plateau; SGG-UGM-2 (2159-order high-precision gravity field model)

## 1. Introduction

The Moho is the interface between the lower crust and the upper mantle. It is an important density interface that marks the boundary between the crust and mantle as well as the gravity compensation interface. It is also the dynamic interface of crust–mantle material exchange and energy exchange. Studying the properties and depth changes of the Moho plays an essential role in understanding the formation and evolution of the crust and mantle, the geodynamic process of the Earth's depth, and the deep structure of the Earth. The Tibetan Plateau (TP) was formed by the collision of the Indian and Eurasian plates. It is the largest and newest orogenic belt in the world; hence, it offers a natural laboratory for studying the dynamics of plate subduction and plateau uplift. Research has shown that the TP is composed of multiple

First author: H. Y. He, hehuiyou@apm.ac.cn
Correspondence to: J. Fang, jfang@whigg.ac.cn
Received 21 FEB 2023; Accepted 06 APR 2023.
Accepted article online 13 JUN 2023.

microplates with tectonic suture zones between the microplates and that faults are widely distributed (Figure 1; Teng JW et al., 1997; Xiong SB and Liu HB, 1997; Wu Y and Gao Y, 2019; Yang WC et al., 2020; Li L et al., 2021; Duan HR et al., 2022; Tan S et al.,2023). The Moho depth records the crustal growth and the geodynamic process experienced by the TP. Through the inversion of the Moho interface, we can understand the huge, thick crust of the TP to further study the deep structure and geodynamic process of the TP (Xiong XS, 2010; Hao TY et al., 2014; He RZ et al., 2014; Hu WJ et al., 2014; Shi QB et al., 2018; Chen YF, 2019; Song T et al., 2020; Zhang GQ et al., 2021; Murodov et al., 2022).

Information on the Moho of the TP can be obtained primarily by gravity and seismic methods. Compared with anomalies in neighboring regions, the Bouguer gravity anomaly in the TP is small and negative, reflecting the thick crust and buried depth of the Moho surface. Following the deployment of the seismic network, increasing amounts of seismic data showed that the Moho surface is deeply buried and that the interior of the TP undergoes complex changes, with drastic changes in the southern margin, relatively gentle changes in the central part, and a steplike uplift in the north. The broadband seismic station describes the variations in Moho characteristics in the TP in detail. The Moho begins to tilt northward from the Himalayas, resulting in a pronounced difference on either side of the Yarlung Zangbo suture zone (IYS). The Moho in the north reaches the maximum depth from the Jinshajiang suture zone (JRS) to the edge of the Qaidam Basin, and then the Moho tilts southward (Liu QM et al., 2014). The deep seismic reflection also provided accurate detection data on the buried depth of the Moho surface of each block in the TP (Gao R et al., 2009; Huang XF et al., 2020; Zhang J et al., 2020). However, seismic exploration focuses on a section or local area, and it was challenging to expand it to cover the entire TP for technical and cost reasons.

Increasingly accurate satellite gravity observation data have become important for inverting the Moho depth of the TP. Combining satellite gravity with seismic methods can invert the global Moho surface structure, reduce the inversion multiplicity, and improve the inversion accuracy (Shin et al., 2009; Dong L et al., 2020; Zhao GD et al., 2020; Avellaneda-Jiménez et al., 2022; Li JB et al., 2022). Inversion of the Moho depth from gravity anomalies is usually done in the spatial domain by linear (Chen WJ and Tenzer, 2017; Chen WJ et al., 2021) or nonlinear (Uieda and Barbosa, 2017) inversion. However, because of the limited computing speed and time required, these methods are impractical for large areas or large volumes of data. The Parker interface inversion method with gravity data in the wavenumber domain is widely used for its rapid calculation speed and high efficiency (Bai YL et al., 2014; Xu C et al., 2017; Shi QB et al., 2018). The method presented herein provides a straightforward means of determining the Moho depth in a given region, though accuracy is heavily reliant upon the discretization of gravity fields and the selection of interface inversion parameters. The latter is particularly crucial, as the precision of prior information regarding the average depth and density variance directly impacts inversion outcomes. To address this, we focused on refining both aspects of our study. Using high-precision satellite gravity anomaly data, the residual gravity anomaly of the Moho was obtained by eliminating the influence of the sedimentary layer and the low-order term of the gravity field via established crustal and gravity field models. Seismic data was then incorporated to further constrain the inversion and obtain accurate parameters. Additionally, to expedite the calculation process and mitigate storage concerns, we utilized the Bott iteration technique in conjunction with the Parker–Oldenburg interface inversion method, resulting in an efficient and highly accurate determination of the Moho depth within the TP.

## 2. Gravity Anomaly of the Moho in the TP

The TP investigated in this work was at 75°E–110°E, 25°W–45°W, the terrain data were SRTM30_ PLUS, its resolution was 30′ × 30′ (Figure 1), the average altitude was more than 5,000 m, and the highest peak, Everest, is 8,848 m above sea level and is located in the Himalayas. Enormous differences are found between the north and south sides of the Himalayas. On the south side is the low-lying the Indo–Gangetic plains. Many peaks in the Himalayas are more than 7,000 m above sea level. Toward the hinterland of the TP, the altitude declines. Low-lying areas, such as the Tarim Basin, Ordos Basin, and Sichuan Basin, formed around the plateau.

The Bouguer gravity anomaly data were from the 2159-order high-precision gravity field model SGG-UGM-2 (Liang W et al., 2020; Ariff et al., 2021). The model used data from the Gravity Field and Steady-State Ocean Circulation Explorer (GOCE), the Gravity Recovery and Climate Experiment (GRACE), satellite altimetry, and the EGM2008 gravity model to solve the resolution of the 5′ × 5′ Earth gravity field model. The model was validated by using a global positioning system (GPS) or leveling data from China and the United States. The accuracy of the SGG-UGM-2 was comparable to that of the authoritative international gravity field model EIGEN-6C4. The accuracy in China was significantly better than that of the EGM2008, and the overall accuracy was better than that of the GOCE model (Figure 2). The Bouguer gravity anomaly in the TP is low and negative, which is different from the anomaly characteristics of the surrounding area. This anomaly is extremely low, mostly below −500 mGal and the lowest value recorded is −675 mGal in the Lhasa block (LSB) and the Qiangtang block (QTB). Obvious abnormal gradient zones occur along the thrust fault at the main front of the Indian plate and Eurasian plate (MFT) and IYS. The Bouguer anomaly of the Qaidam Basin changes gently, while that of Qilian Mountain increases gradually. Among the areas surrounding the TP, the Tarim Basin, the Sichuan Basin, the Ordos Basin, and the Indo–Gangetic plains exhibit higher Bouguer gravity anomalies, with the latter showing particularly high values on the south side of the MFT.

To study the Moho depth, it is necessary to acquire the gravity anomaly resulting from the Moho undulation. To improve the precision of field separation in this study, we directly stripped the gravity response of the sedimentary layer as well as the low-order term of the gravity field from the Bouguer gravity anomaly of the TP. This enabled us to obtain the residual gravity anomaly caused by the Moho. The sedimentary layer data are sourced from CRUST1.0, the latest global crustal model with a precision of 1° × 1°, which is the global Earth model data from ETOPO1 of the

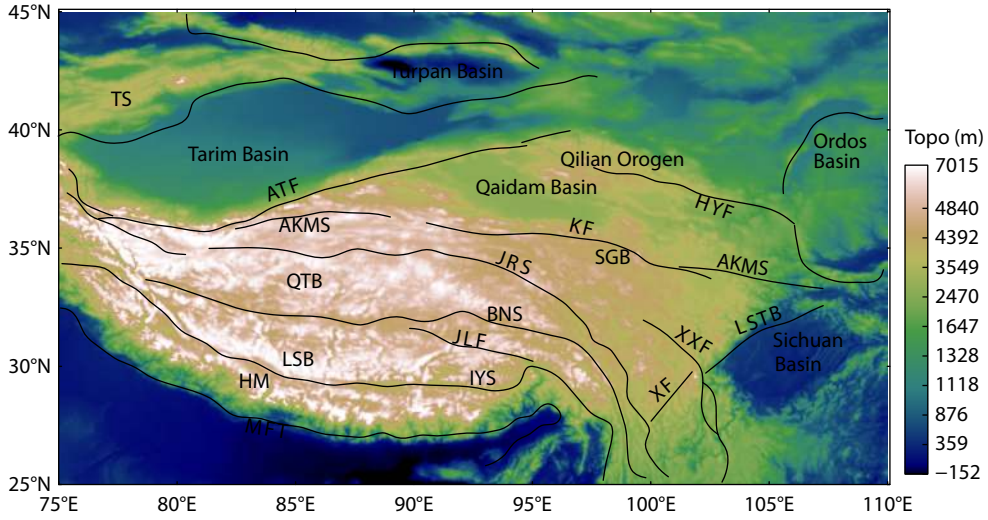


**Figure 1**. Topographic and structural map of the Tibetan Plateau (modified from Bai L et al., 2017; Li W, 2018; Li L et al., 2021). TS, Tianshan; ATF, Altyn Tagh fault; AKMS, Kunlun suture zone; QTB, Qiangtang block; LSB, Lhasa block; HM, Himalayan block; MFT, thrust fault at the main front of the Indian plate and Eurasian plate; KF, Kunlun fault; SGB, Songpan–Garzê block; JRS, Jinshajiang suture zone; BNS, Bangong–Nujiang suture zone; JLF, Jiali fault; IYS, Yarlung Zangbo suture zone; HYF, Haiyuan fault; LSTB, Longmenshan fault; XXF, Xianshuihe–Xiaojiang fault; XF, Xiaojinhe fault.

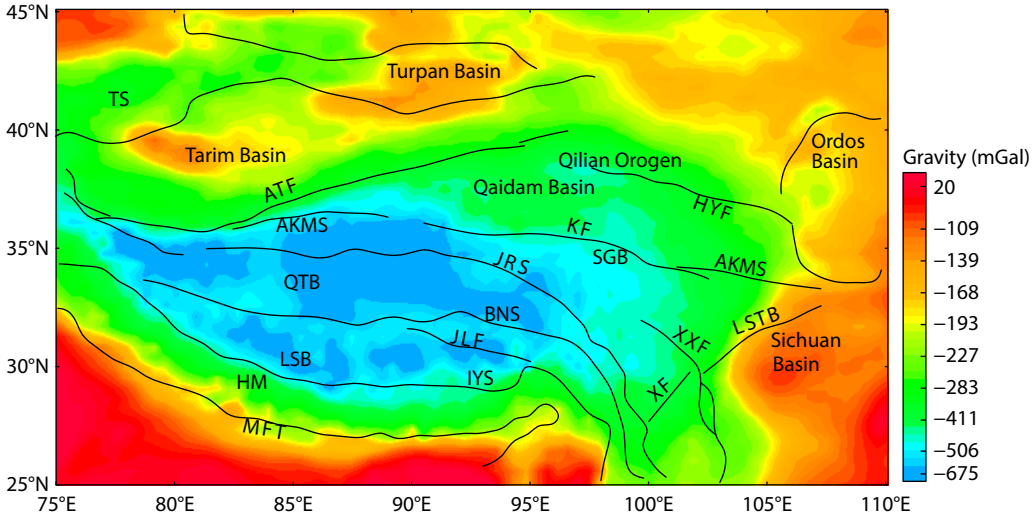


**Figure 2**. Bouguer gravity anomaly of the Tibetan Plateau. TS, Tianshan; ATF, Altyn Tagh fault; AKMS, Kunlun suture zone; QTB, Qiangtang block; LSB, Lhasa block; HM, Himalayan block; MFT, thrust fault at the main front of the Indian plate and Eurasian plate; KF, Kunlun fault; SGB, Songpan–Garzê block; JRS, Jinshajiang suture zone; BNS, Bangong–Nujiang suture zone; JLF, Jiali fault; IYS, Yarlung Zangbo suture zone; HYF, Haiyuan fault; LSTB, Longmenshan fault; XXF, Xianshuihe–Xiaojiang fault; XF, Xiaojinhe fault.

National Oceanic and Atmospheric Administration (Laske et al., 2013; Jiang YT et al., 2014; Luo F et al., 2020). The gravitational response of the sedimentary layer in the TP was calculated by the wavenumber domain forward formula (Figure 3a). Based on Fang J and Xu HZ (2002), the order of gravitational potential spherical harmonic functions of the lower and upper mantle are 2–6 and 7–60, respectively. The gravity field model selected in this work was SGG-UGM-2 (Liang W et al., 2020). The gravity of the long wavelength part corresponded to the 2–60-order spherical harmonic function of the gravity field model (Figure 3b).

The residual gravity anomaly value was determined through field separation techniques (Figure 4), revealing a complex variation in the Moho gravity anomaly that exhibits significant amplitude changes. The gravity anomaly inside the TP is negative, showing a distinct low–high–low–high–low pattern when moving from south to north. The anomaly values in the middle and west of the Songpan-Garzê block (SGB) are low, and the minimum value reaches approximately −551.1 mGal. The Moho gravity anomaly in the TP is significantly lower compared to the surrounding area, creating a noticeable gradient zone. To the south side of the TP, the anomaly decreases sharply from positive to negative as it transitions from the Indian block to the Himalayan block, exhibiting considerable variability that reflects the region's overall anomaly characterization. Conversely, the Moho gravity anomaly values in the Tarim and Sichuan Basins are higher.

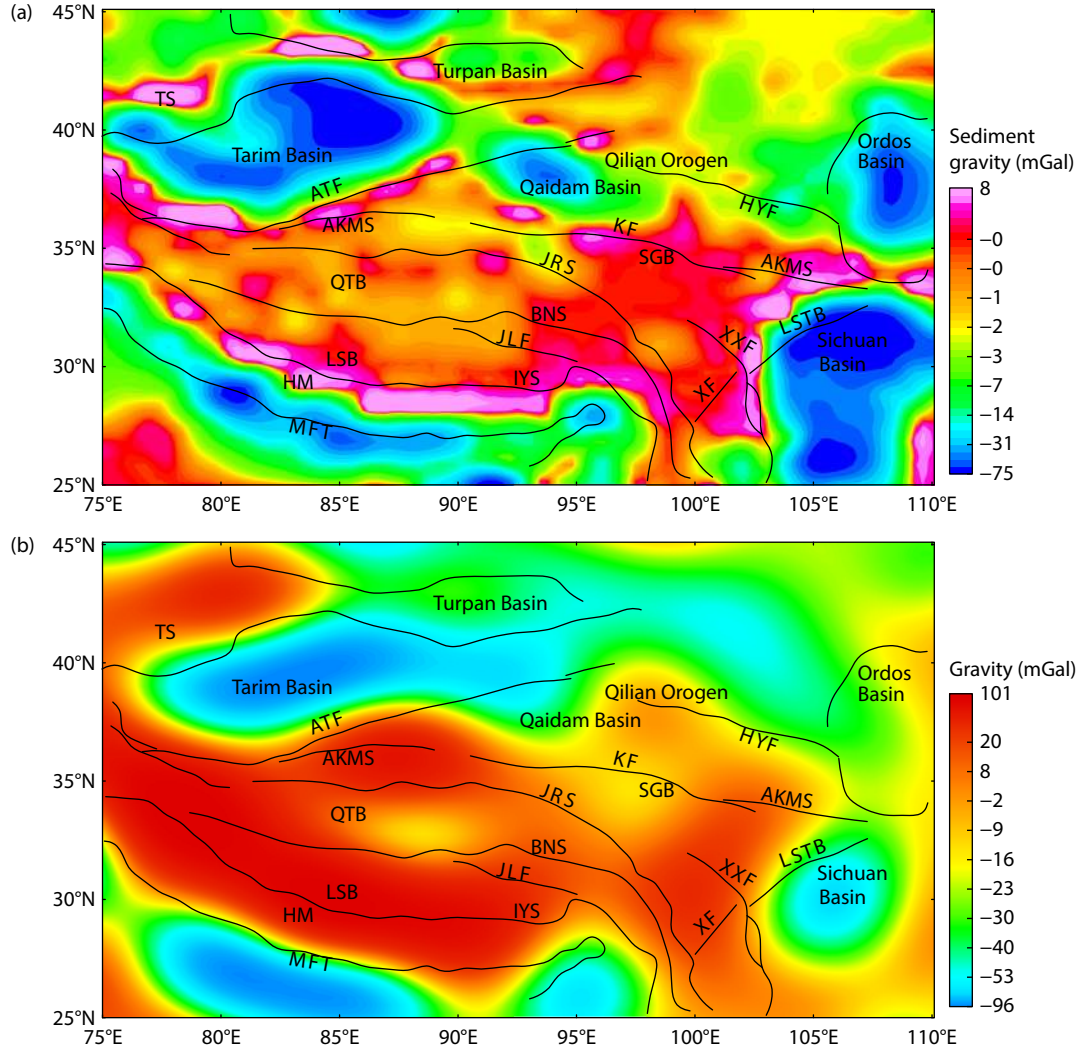


**Figure 3**. The sedimentary layer and low-order term of the gravity field of the Tibetan Plateau. (a) Gravity response of the sedimentary layer; (b) low-order term of the gravity field. TS, Tianshan; ATF, Altyn Tagh fault; AKMS, Kunlun suture zone; QTB, Qiangtang block; LSB, Lhasa block; HM, Himalayan block; MFT, thrust fault at the main front of the Indian plate and Eurasian plate; KF, Kunlun fault; SGB, Songpan–Garzê block; JRS, Jinshajiang suture zone; BNS, Bangong–Nujiang suture zone; JLF, Jiali fault; IYS, Yarlung Zangbo suture zone; HYF, Haiyuan fault; LSTB, Longmenshan fault; XXF, Xianshuihe–Xiaojiang fault; XF, Xiaojinhe fault.

## 3. Moho Depth Inversion

In 1973, Parker introduced a wavenumber domain forward formula that boasts high precision and rapid speed. Subsequently, Oldenburg further developed this concept by proposing a wavenumber domain interface inversion method based on Parker's formula (Parker, 1973; Oldenburg, 1974):

$$F[h(\xi,\eta)] = \frac{F[\Delta g(x,y)]\,\mathrm{e}^{|k|z_0}}{2\pi\gamma}\sum_{n=2}^{\infty}\frac{(-k)^{n-1}}{n!}\left[\rho(\xi,\eta)\,h^n(\xi,\eta)\right], \quad (1)$$

where $F[\ ]$ is the fast Fourier transform, $h(\xi,\eta)$ is the density surface, $\Delta g(x,y)$ is a gravity anomaly, $z_0$ is the average depth, $k$ is the wavenumber, $\rho(\xi,\eta)$ is the density, $\gamma$ represents the gravitational constant, and $n$ denotes the Taylor expansion series. Some scholars have explored methods how to enhance the computational efficiency and precision of interface inversion. To fully exploit the high resolution of the spatial domain and the fast computation of the wavenumber domain, the Bott iteration method is introduced for inversion by integrating both domains (Granser, 1987; Chai YF and Hinze, 1988). This rapid and iterative calculation method, initially proposed by Bott in 1960, is an inversion method for calculating the depth of sedimentary basins based on the gravity anomaly formula of the material layer. In this work, an iterative inversion formula based on the initial value of the interface depth is given (Bott, 1960):

$$h^m(x_i,y_j) = \boldsymbol{h}^{m-1}(x_i,y_j) + \frac{g^{\mathrm{o}}(x_i,y_j) - g\left(x_i,y_j,\Delta\rho,\boldsymbol{h}^{m-1}\right)}{2\pi\gamma\Delta\rho}, \quad (2)$$

where $m$ is the number of iterations, $h^m(x_i,y_j)$ represents the value of $(x_i,y_j)$ for the interface function at the $m$th iteration, $\boldsymbol{h}^{m-1}$ represents the value of the interface function at the $(m-1)$th iteration, $g^{\mathrm{o}}(x_i,y_j)$ is the gravity field observation, $\Delta\rho$ is the density difference, $g\left(x_i,y_j,\Delta\rho,\boldsymbol{h}^{m-1}\right)$ is the theoretical gravity value of the $(m-1)$th iteration of the interface function $\boldsymbol{h}^{m-1}$ forward modeling. The iteration process is terminated when the specified number of iterations is reached or when the fitting difference between the model response and the measured data meets the

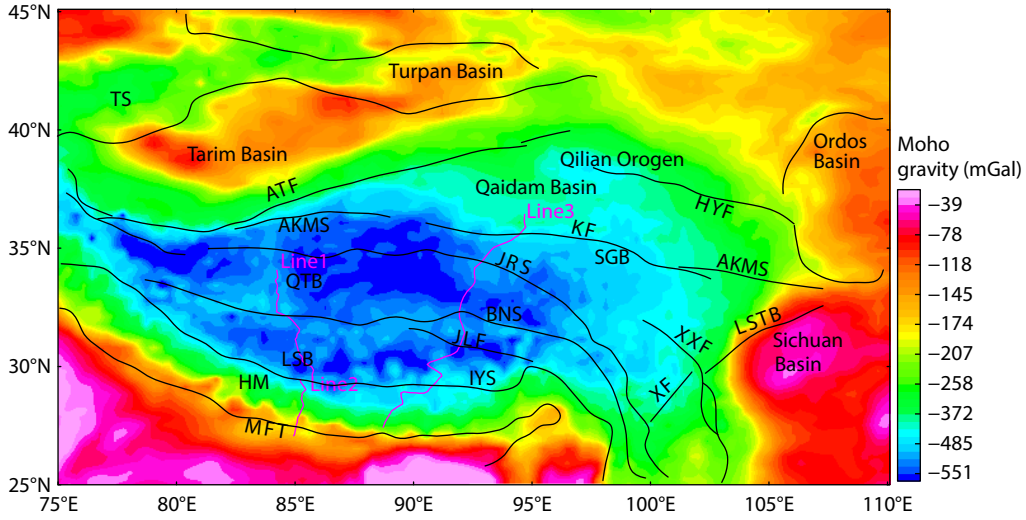


**Figure 4**. The Moho gravity anomaly of the Tibetan Plateau. The purple line is the reference profile: Line1 is the Coqên–Sangehu seismic profile, Line2 is the Zhangmu–Saga–Coqên profile and Line3 is the Yadong–Golmud geoscience section. TS, Tianshan; ATF, Altyn Tagh fault; AKMS, Kunlun suture zone; QTB, Qiangtang block; LSB, Lhasa block; HM, Himalayan block; MFT, thrust fault at the main front of the Indian plate and Eurasian plate; KF, Kunlun fault; SGB, Songpan–Garzê block; JRS, Jinshajiang suture zone; BNS, Bangong–Nujiang suture zone; JLF, Jiali fault; IYS, Yarlung Zangbo suture zone; HYF, Haiyuan fault; LSTB, Longmenshan fault; XXF, Xianshuihe–Xiaojiang fault; XF, Xiaojinhe fault.

accuracy requirement. Silva et al. (2014) extended the Bott iterative algorithm to different density models.

In this study, we set a group of interface models for forward modeling. The calculation range was approximately from −50 to 50 km with an interface fluctuation of 0–4 km and a grid number of 128 × 128. To compare the forward modeling of the gravity anomaly of the interface model, we conducted both spatial and wavenumber domain analyses. Encouragingly, the wavenumber domain forward modeling took only a mere 29 s, a stark contrast to the 1,070 s for the spatial domain, resulting in a significant acceleration of the calculation speed. The Bott iteration formula was introduced into the inversion calculation of the interface model to obtain the interface inversion results in the wavenumber domain. The results of the interface inversion in the wavenumber domain were compared with those of the theoretical model with a maximum residual of 0.017 km, a minimum of −0.02 km, and an average of 0.005 km.

Seismic data have long played a crucial role in exploring the Moho in the TP. Extensive seismic observations and comprehensive studies have been conducted in this region (Gao R et al., 2009; Xiong XS, 2010; Fan J, 2015; Liu Z et al., 2015). The CRUST1.0 Global Crustal Model, released in 2013 with a resolution of 1° × 1°, is the most detailed global crustal model available (Jiang YT et al., 2014; Zhu T, 2016; Luo F et al., 2020). This model provides an invaluable reference value for investigating deep structures in the world. When the inversion of the TP Moho was compared with the depth of the Moho obtained by seismic exploration and the results of the Moho in CRUST1.0, the optimal inversion parameters of interface inversion were obtained by the constraint of seismic data.

Three seismic profiles were extracted as a reference, namely, the Coqên–Sangehu Seismic Profile (Line1; Pan YS and Kong XR, 1998; Teng JW et al., 2002; Zheng D and Yao TD, 2004), the Zhangmu–Saga–Coqên (Line2; Teng JW et al., 2002), and the Yadong–Golmud geoscience section (Line3; Meng LS et al., 1990). These profiles provided average depths (in kilometers) and density differences (in grams per cubic centimeter) of 35/0.45, 37/0.43, 37/0.45, 39/0.43, and 39/0.45, respectively, which were crucial to our analysis. To determine the Moho depth of the Tibetan Plateau, we employed the Bott iteration method and wavenumber domain interface inversion calculation. This approach allowed us to obtain the depth of the TP Moho with a calculation grid number of 89 × 131, 5 iterations, and a calculation time of 1.7 s. The same grid size space-domain calculation required 2,812 s, and the calculation speed was significantly improved.

Seismic profile Line1, Coqên–Sangehu (Figure 5a), provides an artificial seismic profile from Coqên–Dongcuo–Gêrzê–Lugu to the Sangehu in the northern TP. It is used to study the deep crustal structure and tectonics of the northwestern TP. The two-dimensional crustal velocity distribution obtained by seismic observation further confirmed the deep structural characteristics of the Bangong–Nujiang suture zone (BNS). Xiong SB and Liu HB (1997) previously demonstrated that the Moho depth on the south side of the BNS is 75–78 km and 65–68 km on the north side. In this study, the inversion results of the parameter 37/0.45 group were in strong agreement with the Moho depth obtained by seismic data, and the standard deviation of the two residuals was just 2.8 km.

Figure 5b, sourced from the Zhangmu–Saga–Coqên profile (Line 2), presents data on the velocity, depth, and thickness of the crustal layer in the area obtained via seismic analysis. Notably, the crustal thickness gradually increases from south to north, with a significant dislocation occurring below the Yarlung Zangbo River (Teng JW et al., 2002). The inversion results of 37/0.45 were in excellent agreement with seismic data, with a standard deviation

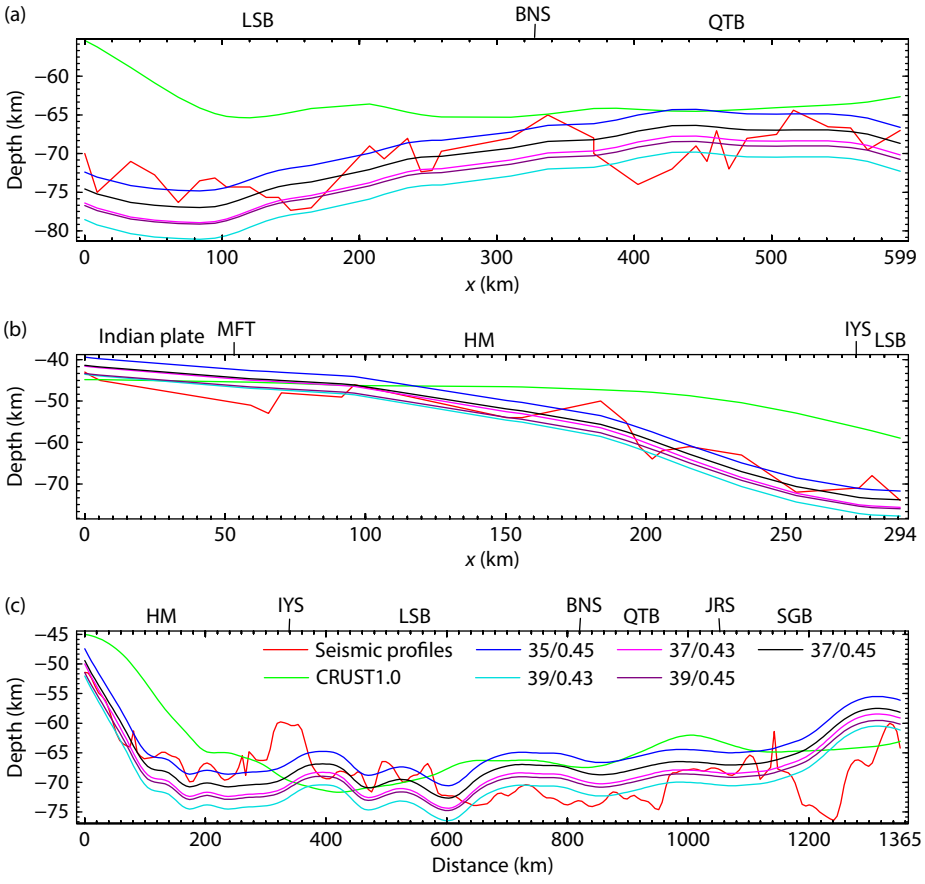


**Figure 5**. Comparison of Moho depths obtained from seismic data and inversion in this study. (a) Line1; (b) Line2; (c) Line3. LSB, Lhasa block; BNS, Bangong–Nujiang suture zone; QTB, Qiangtang block; MFT, thrust fault at the main front of the Indian plate and Eurasian plate; HM, Himalayan block; IYS, Yarlung Zangbo suture zone; JRS, Jinshajiang suture zone; SGB, Songpan–Garzê block.

of only 3.5 km.

Figure 5c illustrates the Yadong–Golmud large lithospheric transect (Line 3) offering valuable insights into geological phenomena such as deep crust division, terrane boundary delineation, and the uplift mechanism of the TP. Meng LS et al. (1990) utilized advanced calculation methods and international processing techniques, in conjunction with the gravity field response and various geophysical and geological data, to propose novel findings. The Moho depth of the Yadong–Golmud survey line is low in the south but high in the north. The shallowest position is at the starting location of Yadong, measuring only 51.4 km, and gradually deepening towards the north. The Moho surface of the LSB exhibits significant variation and reaches a remarkable low of 70 km. Near the IYS, the Moho rises to 60 km, subsequently descending northward to a depth of 72 km within the LSB. The inversion results of 37/0.45 were in good agreement with seismic data, with a standard deviation of only 4.2 km.

In conclusion, the optimal reference average depth was 37 km, and the average density was 0.45 g/cm$^3$, as depicted in Figure 6. The Moho surface of the TP obtained by the interface inversion was forwarded in the wavenumber domain to obtain its forward gravity response (Figure 7a). The resulting gravity anomaly was then compared to the Moho surface gravity anomaly obtained by field separation (Figure 7c). The residual conformed to the normal distribution law, with an average value of −12.45 mGal and a standard deviation of 32 mGal. Our results indicated that the Moho inversion is highly accurate in most areas of the TP's main body, as evidenced by the low amplitude and gentle variation in gravity anomaly residuals. However, the noticeable residuals were found in the areas surrounding the TP, such as the Himalayan block, Tarim Basin, and Sichuan Basin, which may be attributed to parameter selection, such as the density difference and the average depth, during the wavenumber domain interface inversion. The Moho retrieved in this work was consistent with those retrieved by CRUST1.0 (Figure 7b), and the residuals also conform to a normal distribution law (Figure 7d), with a standard deviation of 5.2 km.

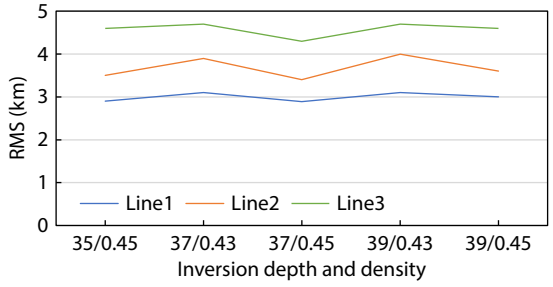


**Figure 6**. The standard deviation of Moho residuals of inversion and seismic or synthetic data. Note: 35/0.45 indicates that the inversion depth is 35 km and the density is 0.45 g/cm$^3$. RMS, root-mean-square.

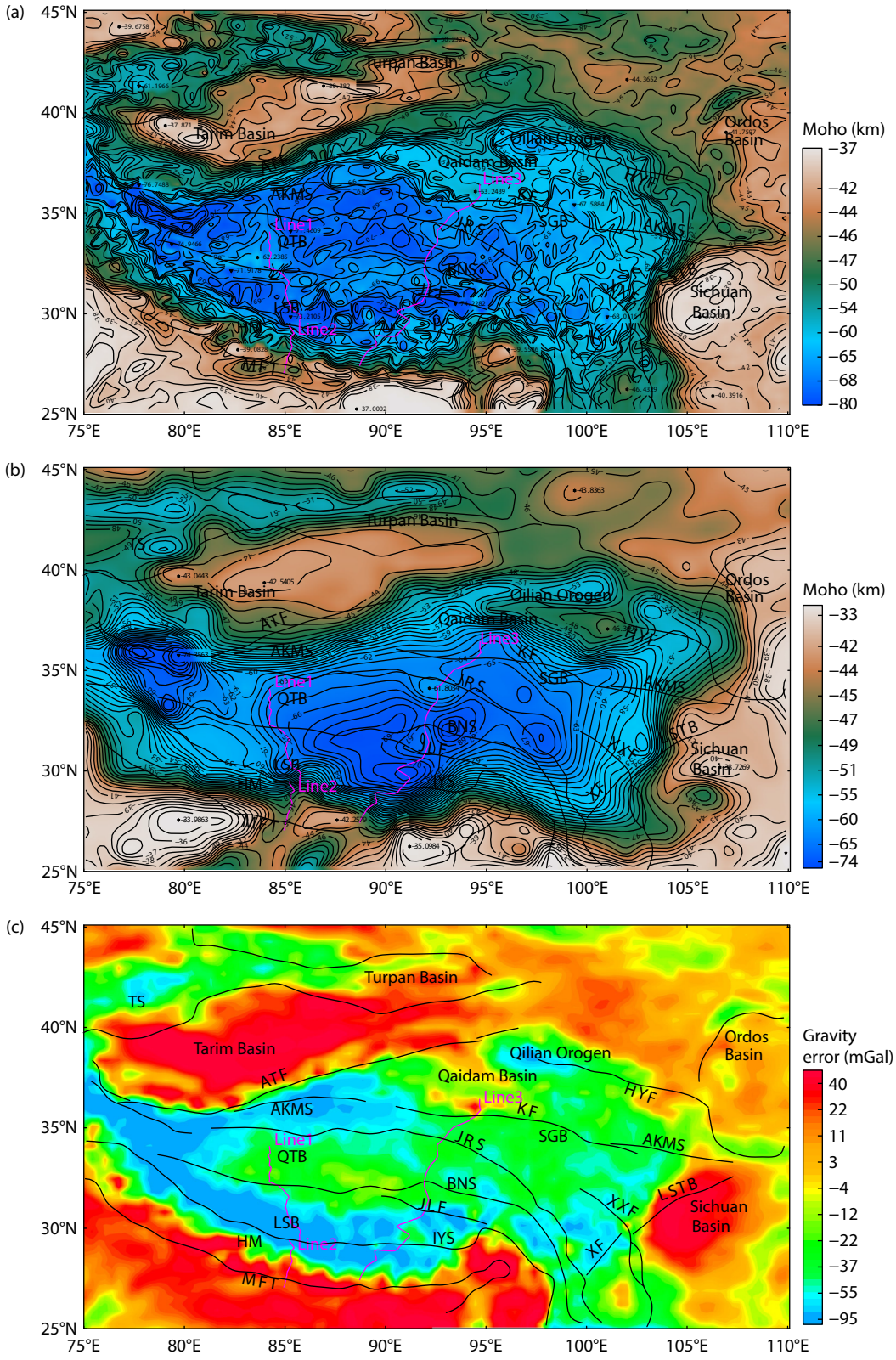
(a)
45°N
40°N
35°N
30°N
25°N
75°E
80°E
85°E
90°E
95°E
100°E
105°E
110°E
Turpan Basin
Tarim Basin
Qilian Orogen
Qaidam Basin
Ordos Basin
Sichuan Basin
TS
ATF
AKMS
QTB
LSB
HM
MFT
KF
JRS
BNS
JLF
IYS
SGB
HYF
XYF
XF
LSTB
Line1
Line2
Line3
Moho (km)
−37
−42
−44
−46
−47
−50
−54
−60
−65
−68
−80
(b)
Moho (km)
−33
−42
−44
−45
−47
−49
−51
−55
−60
−65
−74
(c)
Gravity error (mGal)
40
22
11
3
−4
−12
−22
−37
−55
−95

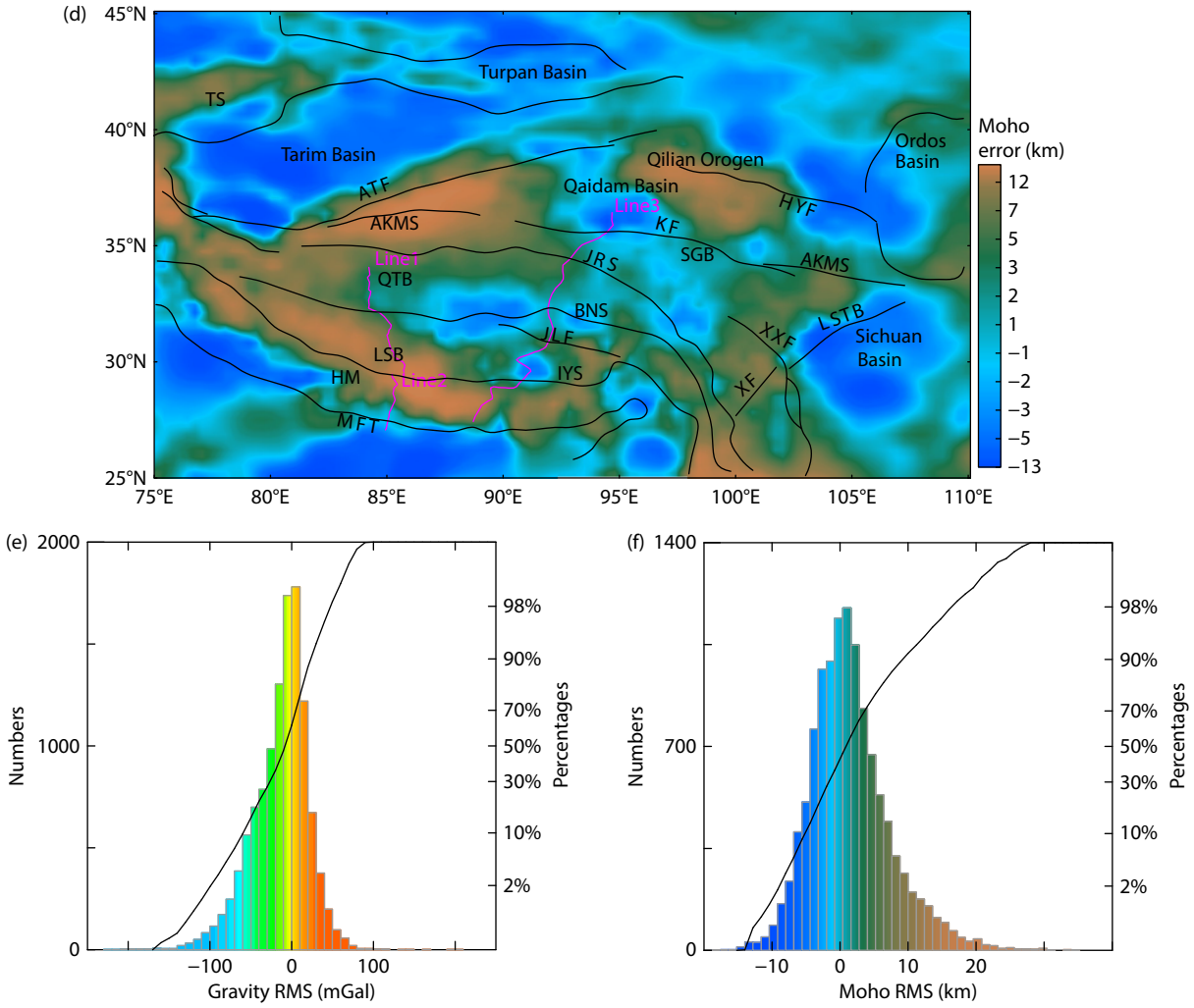


**Figure 7**. The Moho depth of the Tibetan Plateau. (a) The Moho by inversion in this study; (b) the Moho in CRUST1.0; (c) residual of the Moho gravity anomaly obtained by the Moho forward gravity response and field separation; (d) the root-mean-square (RMS) between (a) and (b); (e) the statistical graph of (c); (f) the statistical graph of (d). TS, Tianshan; ATF, Altyn Tagh fault; AKMS, Kunlun suture zone; QTB, Qiangtang block; LSB, Lhasa block; HM, Himalayan block; MFT, thrust fault at the main front of the Indian plate and Eurasian plate; KF, Kunlun fault; SGB, Songpan–Garzê block; JRS, Jinshajiang suture zone; BNS, Bangong–Nujiang suture zone; JLF, Jiali fault; IYS, Yarlung Zangbo suture zone; HYF, Haiyuan fault; LSTB, Longmenshan fault; XXF, Xianshuihe–Xiaojiang fault; XF, Xiaojinhe fault.

## 4. Characteristics of Analysis of the Moho in the TP

The inversion results of the Moho interface in the wavenumber domain revealed that the shape of the Moho surface in the TP and its surrounding areas is complex and that the depth changes significantly. The Moho surface in the interior of the TP is deeply buried. It exhibits the characteristic of two depressions and two uplifts with a relatively gentle trend, where the southwest is low and the northeast is high. It reflects the intense activity in the deep interior of the crust by the mixing action of the northward subduction force of the Indian plate and the blocking force of the hard Alashan block in the north. In contrast, the Moho surface in the surrounding area rises sharply, forming a dense gradient change zone on the TP's edge, particularly as the Moho surface of the Himalayan block changes more violently. The depth of the Moho surface in the Indian plate on the south side is 38 km, while it reaches 74 km in the LSB on the north side, with a range of 37 km. The largest burial depth is in the north of the IYS, with a depth of 80 km, indicating that the northward subduction of the Indian plate may have crossed the IYS.

According to the GPS velocity field study, the crustal movement at the southern margin of the TP exhibits a south-to-north direction, indicating the subduction of the Indian slab towards the Eurasian plate at a rate of 14 mm/a (Wang M and Shen ZK, 2020). The resulting changes to the Moho are significant, particularly on the south side of the IYS, where the Moho inclines northward in line with the IYS and north-to-south extrusion of the Indian and Eurasian plates (Royden et al., 2008). The Moho of the LSB on the north side of the IYS experiences depression, forming a low-lying area of the Moho in the TP with a depth of 65–76 km. Seismic exploration shows that the Indian plate dips northward from 40 km below the Ganga basin to a depth of 50 km below the Himalayan block and continues to subduct northward below the LSB to a depth of 70 km near 31°N (Nábělek et al., 2009), which is

consistent with our inversion results. The Moho surface uplifts on the south side of the QTB and the north side of the LSB, gracefully tilting southward in alignment with the BNS. The Moho of the QTB in the central TP is the shallowest and uplifting, and the crust is thinning. Tseng et al. (2009) detected by seismic means that the crust beneath the QTB thinned to 60 km, which also verified our results. The Moho in the QTB trends nearly east–west trending, whereas it is northwest trending in the west, which reflects the northward subduction of the Indian plate and resulting deformation and uplift of the TP. The hard Tarim Basin to the north forms a significant barrier, resulting in the formation of the ATF and severe deformation of the TP's crust. The Moho changes along the ATF.

In the northwest Tarim Basin, the Moho depth is shallowest at 38 km, gradually rising to 45 km on both sides. The Moho of the SGB exhibits a west-to-east increase in depth. A rise–fall–rise pattern characterizes the Moho from the Qaidam Basin to the northeast. The Moho of the South Qilian terrane has a lower depth of about 66 km than that of the surrounding regions. The Moho of the Ordos Basin reaches 42 km, effectively blocking the northeastern margin of the TP. GPS measurements reveal gradual crustal deformation and a decrease in crustal velocity. The Moho surface displays an apparent gradient zone at the boundary, which uplifts to the Ordos Basin (Wang M and Shen ZK, 2020). The Moho on both sides of the Longmenshan fault (LSTB) exhibits a significantly nearly north–south variation. The east side is the Sichuan Basin, whose Moho is highest in the middle and lowest at the periphery, reaching a maximum of 38 km. An obvious variation belt exists between the Sichuan Basin and the SGB. Along the Xianshuihe–Xiaojiang fault (XXF), the Moho contour extends southward. The Moho contour has an apparent gradient zone at the TP boundary, consistent with the main fault direction's rotation and the GPS velocity field's changing trend (Zheng G et al., 2017).

The results of this study were compared with those of previous studies (Figure 8 and Table 1). The observed variation in the Moho depth across the TP exhibits a remarkable consistency. Our results show a standard deviation of only 3.45 km, which is in close agreement with the Moho depth estimated by the INDEPTH-III project (International Deep Profiling of Tibet and the Himalaya; Tian XB et al., 2005). Moreover, the Moho depth range in the TP microplates is consistent with previous research results (Table 1).

This analysis provided a clearer understanding of the geodynamic process of the TP (Figure 9). Multiple data points confirmed the continuation of the Himalayan movement, which triggered the TP uplift. Since the Eocene, the TP has undergone a complex uplift process, characterized by a balance between uplift and erosion, tectonic uplift and balanced uplift, and the alternation between slow uplift and rapid uplift (Hou ZQ et al., 2021). The Indian plate subducted the Eurasian plate from south to north, forming the main boundary fault on the southern side of the Himalayas, thus providing direct energy for the uplift of the TP. Simultaneously, the plateau is subject to the resistance of the Eurasian plate and the north–south thrust of the Qaidam Basin plate, leading to rapid deformation and uplift. Subsequently, the continental collision and intracontinental subduction have successively formed several thrust-overlapping structures and thickened the crust. The crustal thickness of the main part of the TP is approximately 70 km deep, twice that of an ordinary continent. However, the crustal thickness of the towering Himalayan block is only approximately 50 km, indicating that the area has not yet reached an equilibrium state of gravity compensation. The north–south, and northeast–south-

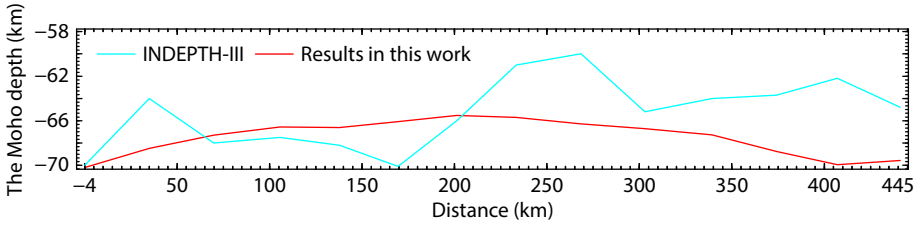


**Figure 8**. The Moho depth by the INDEPTH-III model. Note: The root-mean-square of seismic and gravity results is 3.35 km.

**Table 1.** Comparison of Moho inversion results with previous results (in kilometers).[a]

| References | Method | Deepest position and depth | HM | LSB | QTB | SGB |
|---|---|---|---|---|---|---|
| Braitenberg et al. (2000) | Gravity | Western, 80 | 45–65 | 70–80 | 70–75 | 60–70 |
| Laske et al. (2013) | Seismic | Western, 74 | 37–55 | 55–70 | 66–71 | 61–69 |
| Shin et al. (2015) | Gravity | Western, 82 | 40–65 | 62–72 | 63–72 | 59–69 |
| Xuan SB and Jin SG (2022) | Gravity | Central, 75.1 | 45–70 | 62–75 | 63–74 | 62–69 |
| In this article | Gravity | Western, 80 | 40–65 | 65–76 | 69–72 | 64–71 |

[a]The gravity data in Braitenberg et al. (2000) is 10′ × 10′ using an iterative hybrid spectral–classical inversion method. The Moho from CRUST1.0 is shown in Laske et al. (2013), which is 1° × 1°. The Moho depths in Shin et al. (2015) and Xuan SB and Jin SG (2022) are inverted by gravity, using the Parker–Oldenburg method with GO_CONS_GCF_2_DIR_R5 (300°) and WGM2012 (which is 0.1° × 0.1°). HM, Himalayan block; LSB, Lhasa block; QTB, Qiangtang block; SGB, Songpan–Garzê block.

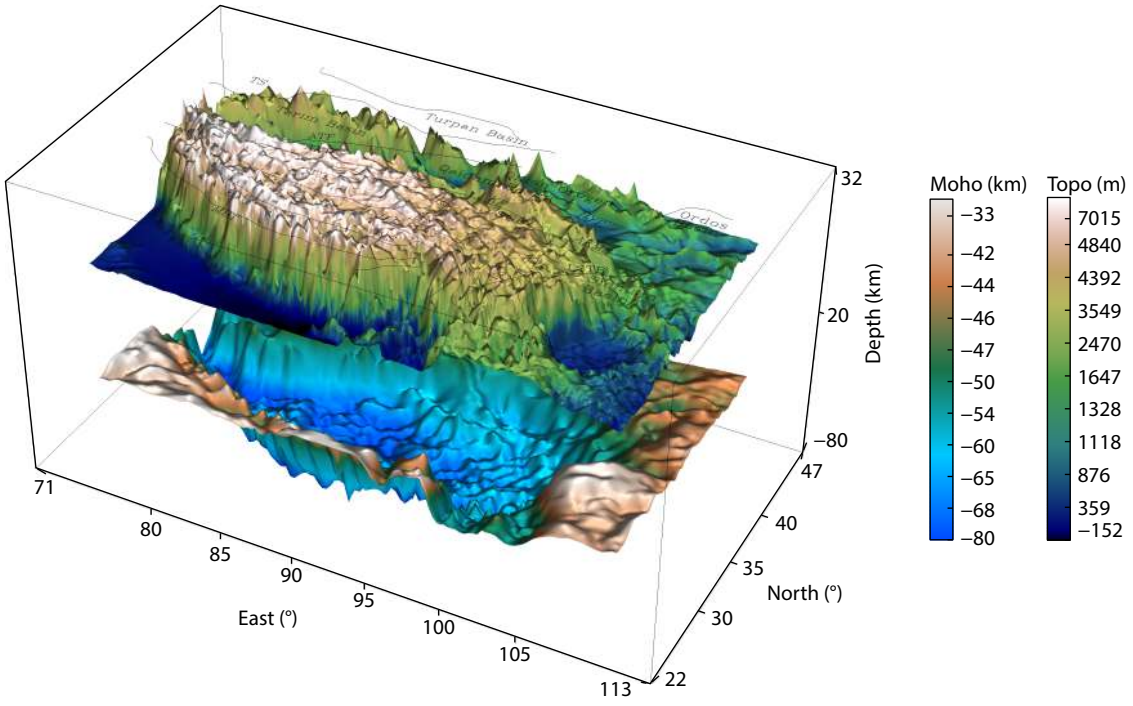


**Figure 9**. The topography and Moho of the Tibetan Plateau.

west horizontal stress field still controls the plateau. Since the collision of the two plates, the northward movement of the Indian plate has remained continuous, and the trend of plateau uplift persists. Zheng G et al. (2017) obtained the Earth slip rate of the main faults in the TP, by inverting the continuous velocity field and the strain rate field, using 2,576 velocity values measured between 1991 and 2015. The NNE crustal shortening rate is approximately 28 mm/a, and the NWW crustal uplift rate is approximately 25 mm/a. The velocity field reveals several undeformed regions, strain concentration regions around major faults, diffusion strain regions, and plateau expansion in the TP and its adjacent areas (Xu CJ, 2002).

## 5. Conclusions

In this work, we determined the Moho in the TP, using high-precision satellite gravity field data and multiple seismic profile information. Using existing crustal and gravity field models, we obtained the local gravity anomaly caused by the Moho surface by stripping out the gravity response of the sedimentary layer and the low-order term of the gravity field caused by the mantle and below. To minimize the multiplicity of gravity inversion, we incorporated three seismic profile information to ascertain the optimal inversion parameters, executed an interface inversion in the wavenumber domain, and employed the Bott iteration. Our results revealed complex variations in the Moho in the TP, in stark contrast to the surrounding areas. The marginal area exhibits a dense gradient zone consistent with the direction of the boundary fault, ranging from 37–45 km to approximately 60–80 km inside the TP. At the southern margin of the TP, the Indian plate has subducted northward, resulting in a northward tilt of the Moho. The hard Tarim Basin, Alashan terrane, Ordos Basin, and Sichuan Basin have slowed the crustal movement on the northwestern, northern, northeastern, and eastern sides (Wang M and Shen ZK, 2020). The Moho tilts to the northeast, south, southwest, and west, respectively. The thickening of the crust in the TP has deepened and rotated the Moho, with its direction orthogonal to the observed deformation rate by the GPS. The Moho surface in the TP is characterized by two depressions and two uplifts, with apparent depressions formed on the north side of the LSB and the QTB. This result may signify the northward subduction of the Indian plate to the Eurasian plate and the southward subduction of the Asian lithosphere (Zhao WJ et al., 2011). The uplift of the Moho surface and the thinning of the crust in the central QTB may be a balanced compensation for the low-density and low-velocity mantle (Nábělek et al., 2009). The uplift of the Moho in the Qaidam Basin may be caused by the weak crust of the TP being injected into the harder Qaidam terrane, indicating the northward development of the TP (Karplus et al., 2011).

## Acknowledgments

This work was financially supported by the National Natural Science Foundation of China (Grant No. 42192535), the Open Fund of Wuhan, Gravitation and Solid Earth Tides, National Observation and Research Station (No. WHYWZ202204), the Strategic Pioneer Science and Technology Special Project of the Chinese Academy of Sciences (Grant No. XDB18010304), and the National Natural Science Foundation of China (Grant No. 41874096). We are grateful to the editors and reviewers for their constructive comments and suggestions, which have helped us improve the manuscript. Thanks are extended to the entire Division of Seismology and Physics in the Earth's Interior team at the Innovation Academy for Precision Measurement Science and Technology.

## References

Ariff, N. S. E., Olesen, A. K., Yaacob, N. M., and Sulaiman, S. A. H. (2021). Evaluation of gravity anomaly and geoid height derived from various

global geopotential model. In *IEEE 12th Control and System Graduate Research Colloquium (ICSGRC)* (pp. 34–39). Shah Alam, Malaysia: IEEE. https://doi.org/10.1109/ICSGRC53186.2021.9515205

Avellaneda-Jiménez, D. S., Monsalve, G., León, S., and Gómez-García, A. M. (2022). Insights into Moho depth beneath the northwestern Andean region from gravity data inversion. *Geophys. J. Int.*, *229*(3), 1964–1977. https://doi.org/10.1093/gji/ggac041

Bai, L., Li, G. H., Khan, N. G., Zhao, J. M., and Ding, L. (2017). Focal depths and mechanisms of shallow earthquakes in the Himalayan–Tibetan region. *Gondwana Res.*, *41*, 390–399. https://doi.org/10.1016/j.gr.2015.07.009

Bai, Y. L., Williams, S. E., Müller, R. D., Liu, Z., and Hosseinpour, M. (2014). Mapping crustal thickness using marine gravity data: methods and uncertainties. *Geophysics*, *79*(2), G27–G36. https://doi.org/10.1190/geo2013-0270.1

Bott, M. H. P. (1960). The use of rapid digital computing methods for direct gravity interpretation of sedimentary basins. *Geophys. J. Int.*, *3*(1), 63–67. https://doi.org/10.1111/j.1365-246X.1960.tb00065.x

Braitenberg, C., Zadro, M., Fang, J., Wang, Y., and Hsu, H. T. (2000). The gravity and isostatic Moho undulations in Qinghai–Tibet plateau. *J. Geodyn.*, *30*(5), 489–505. https://doi.org/10.1016/s0264-3707(00)00004-1

Chai, Y. F., and Hinze, W. J. (1988). Gravity inversion of an interface above which the density contrast varies exponentially with depth. *Geophysics*, *53*(6), 837–845. https://doi.org/10.1190/1.1442518

Chen, W. J., and Tenzer, R. (2017). Moho modeling in spatial domain: a case study under Tibet. *Adv. Space Res.*, *59*(12), 2855–2869. https://doi.org/10.1016/j.asr.2017.03.015

Chen, W. J., Tenzer, R., Xu, X. Y., Wang, S., and Wang, B. (2021). Moho depth estimation beneath Tibet from satellite gravity data based on a condensation approach. *Earth Space Sci.*, *8*(6), e2020EA001261. https://doi.org/10.1029/2020EA001261

Chen, Y. F. (2019). Research of lithospheric discontinuity structure beneath NE Tibetan Plateau from receiver function (in Chinese) [Ph. D. thesis]. Beijing: Institute of Geology, China Earthquake Administration. https://doi.org/10.27489/d.cnki.gzdds.2019.000009

Dong, L., Shen, X. Z., and Qian, Y. P. (2020). Study on velocity and density contrasts across the Moho in the southeastern margin of the Tibetan Plateau. *Chin. J. Geophys.* (*in Chinese*), *63*(3), 915–927. https://doi.org/10.6038/cjg2020N0168

Duan, H. R., Guo, J. G., Chen, L. K., Jiao, J. S., and Jian, H. T. (2022). Vertical crustal deformation velocity and its influencing factors over the Qinghai–Tibet Plateau based on satellite gravity data. *Earth Planet. Phys.*, *6*(4), 366–377. https://doi.org/10.26464/epp2022034

Fan, J. (2015). Study the structure of crust and upper mantle in eastern margin of Qinghai–Tibet plateau and western margin of Yangtze platform by a seismological passive source experiment (in Chinese) [Ph. D. thesis]. Chengdu: Chengdu University of Technology.

Fang, J., and Xu, H. Z. (2002). A study of the depth of geoid anomaly sources in China and its adjacent regions. *Chin. J. Geophys.* (*in Chinese*), *45*(1), 42–48.

Gao, R., Xiong, X. S., Li, Q. S., and Lu, Z. W. (2009). The Moho depth of Qinghai–Tibet plateau revealed by seismic detection. *Acta Geosci. Sin.* (*in Chinese*), *30*(6), 761–773. https://doi.org/10.3975/cagsb.2009.06.08

Granser, H. (1987). Nonlinear inversion of gravity data using the Schmidt–Lichtenstein approach. *Geophysics*, *52*(1), 88–93. https://doi.org/10.1190/1.1442243

Hao, T. Y., Hu, W. J., Xing, J., Hu, L. T., Xu, Y., Qin, J. X., Liu, S. H., and Lei, S. M. (2014). The Moho depth map (1:5000000) in the land and seas of China and adjacent areas and its geological implications. *Chin. J. Geophys.* (*in Chinese*), *57*(12), 3869–3883. https://doi.org/10.6038/cjg20141202

He, R. Z., Shang, X. F., Yu, C. Q., Zhang, H. J., and van der Hilst, R. D. (2014). A unified map of Moho depth and $V_P/V_S$ ratio of continental China by receiver function analysis. *Geophys. J. Int.*, *199*(3), 1910–1918. https://doi.org/10.1093/gji/ggu365

Hou, Z. Q., Xu, B., Zheng, Y. C., Zheng, H. W., and Zhang, H. R. (2021). Mantle flow: the deep mechanism of large-scale growth in Tibetan Plateau. *Chin. Sci. Bull.* (*in Chinese*), *66*(21), 2671–2690. https://doi.org/10.1360/TB-2020-0817

Hu, W. J., Hao, T. Y., Qin, J. X., Li, Z. W., Jiang, W. W., Jiang, D. D., Xing, J., Hu, L. T., Xu, Y., and Lei, S. M. (2014). Moho depth and deep crustal structure in the land and seas of China and adjacent areas: an example of the Altay–Bashi channel profile. *Chin. J. Geophys.* (*in Chinese*), *57*(12), 3932–3943. https://doi.org/10.6038/cjg20141207

Huang, X. F., Xu, X., Gao, R., Guo, X. Y., and Li, W. H. (2020). Shortening of lower crust beneath the NE Tibetan Plateau. *J. Asian Earth Sci.*, *198*, 104313. https://doi.org/10.1016/j.jseaes.2020.104313

Jiang, Y. T., Zhang, Y. Z., Wang, S., and Wei, Y. M. (2014). The lithospheric heterogenities of China mainland and neighborhood based on CRUST1.0 and its characteristics. *J. Geod. Geodyn.* (*in Chinese*), *34*(6), 60–65. https://doi.org/10.14075/j.jgg.2014.06.012

Karplus, M. S., Zhao, W., Klemperer, S. L., Wu, Z., Mechie, J., Shi, D., Brown, L. D., and Chen, C. (2011). Injection of Tibetan crust beneath the south Qaidam Basin: evidence from INDEPTH IV wide-angle seismic data. *J. Geophys. Res.*: *Solid Earth*, *116*(B7), B07301. https://doi.org/10.1029/2010JB007911

Laske, G., Masters, G., Ma, Z. T., and Pasyanos, M. (2013). Update on CRUST1.0—A 1-degree global model of Earth's crust. In *EGU General Assembly*. Vienna: EGU.

Li, J. B., Xu, C., and Chen, H. P. (2022). An improved method to Moho depth recovery from gravity disturbance and its application in the South China Sea. *J. Geophys. Res.*: *Solid Earth*, *127*(7), e2022JB024536. https://doi.org/10.1029/2022JB024536

Li, L., Zhang, X. Z., Liao, J., Liang, Y. L., and Dong, S. X. (2021). Geophysical constraints on the nature of lithosphere in central and eastern Tibetan Plateau. *Tectonophysics*, *804*, 228722. https://doi.org/10.1016/j.tecto.2021.228722

Li, W. (2018). Study on gravity inversion and seismogenic environment of density in Tibetan Plateau and its adjacent areas (in Chinese) [Ph. D. thesis]. Wuhan: Wuhan University.

Liang, W., Li, J. C., Xu, X. Y., Zhang, S. J., and Zhao, Y. Q. (2020). A high-resolution earth's gravity field model SGG-UGM-2 from GOCE, GRACE, satellite altimetry, and EGM2008. *Engineering*, *6*(8), 860–878. https://doi.org/10.1016/j.eng.2020.05.008

Liu, Q. M., Zhao, J. M., Lu, F., and Liu, H. B. (2014). Crustal structure of northeastern margin of the Tibetan Plateau by receiver function inversion. *Sci. China Earth Sci.*, *57*(4), 741–750. https://doi.org/10.1007/s11430-013-4772-5

Liu, Z., Tian, X. B., Liang, X. F., and Teng, J. W. (2015). Upper mantle structure beneath central Tibet derived from teleseismic S wave tomography along the INDEPTH-III profile. *Chin. J. Geophys.* (*in Chinese*), *58*(4), 1169–1178. https://doi.org/10.6038/cjg20150407

Luo, F., Yan, J. Y., Fu, G. M., Luo, L., Tao, X., and Wang, H. (2020). CRUST 1.0 crustal model and its application: an example from middle-lower Yangtze metallogenic belt. *Acta Geosci. Sin.* (*in Chinese*), *94*(2), 648–660. https://doi.org/10.19762/j.cnki.dizhixuebao.2019134

Meng, L. S., Gao, R., Zhou, F. X., Li, L., and Wang, H. X. (1990). Interpretation of the crustal structure in Yadong–Golmud area using gravity anomalies. *Bull. Chin. Acad. Geol. Sci.* (*in Chinese*), *21*(2), 149–161.

Murodov, D., Mi, W., Murodov, A., Oimuhmmadzoda, I., Abdulov, S., and Xin, W. (2022). Deep crustal structure beneath the Pamir–Tibetan Plateau: insights from the Moho depth and $V_P/V_S$ ratio variation. *Front. Earth Sci.*, *10*, 821497. https://doi.org/10.3389/feart.2022.821497

Nábělek, J., Hetényi, G., Vergne, J., Sapkota, S., Kafle, B., Jiang, M., Su, H. P., Chen, J., Huang, B. S., and Team, T. H. C. (2009). Underplating in the Himalaya–Tibet collision zone revealed by the Hi-CLIMB experiment. *Science*, *325*(5946), 1371–1374. https://doi.org/10.1126/science.1167719

Oldenburg, D. W. (1974). The inversion and interpretation of gravity anomalies. *Geophysics*, *39*(4), 526–536. https://doi.org/10.1190/1.1440444

Pan, Y. S., and Kong, X. R. (1998). *Lithosphere Structure, Evolution and Dynamics of Qinghai–Xizang (Tibetan) Plateau* (in Chinese). Guangzhou: Guangdong Science & Technology Press, 3–13.

Parker, R. L. (1973). The rapid calculation of potential anomalies. *Geophys. J. Int.*, *31*(4), 447–455. https://doi.org/10.1111/j.1365-246X.1973.tb06513.x

Royden, L. H., Burchfiel, B. C., and van der Hilst, R. D. (2008). The geological evolution of the Tibetan Plateau. *Science*, *321*(5892), 1054–1058. https://doi.

org/10.1126/science.1155371

Shi, Q. B., Hu, S. G., and Yang, L. (2018). Inversion of Moho depth in Tibetan Plateau based on high-precision satellite gravity data. *Chin. J. Eng. Geophys.* (*in Chinese*), *15*(4), 466–474. https://doi.org/10.3969/j.issn.1672-7940.2018.04.011

Shin, Y. H., Shum, C. K., Braitenberg, C., Lee, S. M., Xu, H. Z., Choi, K. S., Baek, J. H., and Park, J. U. (2009). Three-dimensional fold structure of the Tibetan Moho from GRACE gravity data. *Geophys. Res. Lett.*, *36*(1), L01302. https://doi.org/10.1029/2008GL036068

Shin, Y. H., Shum, C. K., Braitenberg, C., Lee, S. M., Na, S. H., Choi, K. S., Hsu, H., Park, Y. S., and Lim, M. (2015). Moho topography, ranges and folds of Tibet by analysis of global gravity models and GOCE data. *Sci. Rep.*, *5*, 11681. https://doi.org/10.1038/srep11681

Silva, J. B. C., Santos, D. F., and Gomes, K. P. (2014). Fast gravity inversion of basement relief. *Geophysics*, *79*(5), G79–G91. https://doi.org/10.1190/geo2014-0024.1

Song, T., Shen, X. Z., and Mei, X. P. (2020). Constraining Moho characteristics with frequency-dependence of receiver function and its application. *Acta Seismol. Sin.* (*in Chinese*), *42*(2), 135–150. https://doi.org/10.11939/jass.20190149

Tan, S., Tian, X., Zeng, X., Nie, F., Qu, C., and Yu, C. (2023). Crustal structure beneath the northern part of the southeastern Tibetan Plateau revealed by a seismic dense nodal array. *J. Asian Earth Sci*, 105593. https://doi.org/10.1016/j.jseaes.2023.105593

Teng, J. W., Xiong, S. B., and Zhang, Z. J. (1997). Review and prospects for geophysical study of the deep lithosphere structure and tectonics in Qinghai–Xizang(Tibet) Plateau. *Chin. J. Geophys.* (*in Chinese*), *40*(S1), 121–139.

Teng, J. W., Zeng, R. S., Yan, Y. F., and Zhang, H. (2002). Depth distribution of Moho and tectonic framework in eastern Asian continent and its adjacent ocean areas. *Sci. China* (*Ser. D*), *46*(5), 428–446. https://doi.org/10.1360/03yd9038

Tian, X. B., Wu, Q. J., Zhang, Z. J., Teng, J. W., and Zeng, R. S. (2005). Joint imaging by teleseismic converted and multiple waves and its application in the INDEPTH-III passive seismic array. *Geophys. Res. Lett.*, *32*(21), L21315. https://doi.org/10.1029/2005gl023686

Tseng, T. L., Chen, W. P., and Nowack, R. L. (2009). Northward thinning of Tibetan crust revealed by virtual seismic profiles. *Geophys. Res. Lett.*, *36*(24), L24304. https://doi.org/10.1029/2009GL040457

Uieda, L., and Barbosa, V. C. F. (2017). Fast nonlinear gravity inversion in spherical coordinates with application to the South American Moho. *Geophys. J. Int.*, *208*(1), 162–176. https://doi.org/10.1093/gji/ggw390

Wang, M., and Shen, Z. K. (2020). Present-day crustal deformation of continental China derived from GPS and its tectonic implications. *J. Geophys. Res.*: *Solid Earth*, *125*(2), e2019JB018774. https://doi.org/10.1029/2019JB018774

Wu, Y., and Gao, Y. (2019). Gravity pattern in southeast margin of Tibetan Plateau and its implications to tectonics and large earthquakes. *Earth Planet. Phys.*, *3*(5), 425–434. https://doi.org/10.26464/epp2019044

Xiong, S. B., and Liu, H. B. (1997). Crustal structure in western Tibetan Plateau. *Chin. Sci. Bull.*, *42*(8), 665–669. https://doi.org/10.1007/BF03182647

Xiong, X. S. (2010). Moho depth and variation of the continent in China and its geodynamic implications (in Chinese) [Ph. D. thesis]. Beijing: Chinese Academy of Geological Sciences.

Xu, C., Liu, Z. W., Luo, Z. C., Wu, Y. H., and Wang, H. H. (2017). Moho topography of the Tibetan Plateau using multi-scale gravity analysis and its tectonic implications. *J. Asian Earth Sci.*, *138*, 378–386. https://doi.org/10.1016/j.jseaes.2017.02.028

Xu, C. J. (2002). *The Kinematic Models of Crustal Movement and Tectonic Stress Field in the Tibetan Plateau* (in Chinese). Beijing: Surveying and Mapping Publishing House.

Xuan, S. B., and Jin, S. G. (2022). Moho depth and crustal density structure in the Tibetan Plateau from gravity data modelling. *J. Asian Earth Sci.*, *233*, 105261. https://doi.org/10.1016/j.jseaes.2022.105261

Yang, W. C., Jin, S., Zhang, L. L., Qu, C., Hu, X. Y., Wei, W. B., Yu, C. Q., and Yu, P. (2020). The three-dimensional resistivity structures of the lithosphere beneath the Qinghai–Tibet Plateau. *Chin. J. Geophys.* (*in Chinese*), *63*(3), 817–827. https://doi.org/10.6038/cjg2020N0197

Zhang, G. Q., Shen, W. B., Fu, G. Y., Li, Z. J., Zhu, Y. Q., and Wang, Y. (2021). Moho changes beneath the northeastern Tibetan Plateau revealed by multiple geodetic datasets. *J. Geophys. Res.*: *Solid Earth*, *126*(11), e2021JB022060. https://doi.org/10.1029/2021JB022060

Zhang, J., Yang, G. L., Tan, H. B., Wu, G. J., and Wang, J. P. (2020). Inversion of Moho surface depth in Sichuan–Yunnan area based on the constraint of receiving function. *Chin. J. Geophys.* (*in Chinese*), *63*(7), 2579–2591. https://doi.org/10.6038/cjg2020N0441

Zhao, G. D., Liu, J. X., Chen, B., Kaban, M. K., and Zheng, X. Y. (2020). Moho beneath Tibet based on a joint analysis of gravity and seismic data. *Geochem. Geophys. Geosyst.*, *21*(2), e2019GC008849. https://doi.org/10.1029/2019GC008849

Zhao, W. J., Kumar, P., Mechie, J., Kind, R., Meissner, R., Wu, Z. H., Shi, D. N., Su, H. P., Xue, G. Q., … Tilmann, F. (2011). Tibetan plate overriding the Asian plate in central and northern Tibet. *Nature Geosci.*, *4*(12), 870–873. https://doi.org/10.1038/NGEO1309

Zheng, D., and Yao, T. D. (2004). Progress in research on formation and evolution of Tibetan Plateau with its environment and resource effects. *China Basic Sci.* (*in Chinese*), *6*(2), 15–21. https://doi.org/10.3969/j.issn.1009-2412.2004.02.003

Zheng, G., Wang, H., Wright, T. J., Lou, Y. D., Zhang, R., Zhang, W. X., Shi, C., Huang, J. F., and Wei, N. (2017). Crustal deformation in the India–Eurasia collision zone from 25 years of GPS measurements. *J. Geophys. Res.*: *Solid Earth*, *122*(11), 9290–9312. https://doi.org/10.1002/2017jb014465

Zhu, T. (2016). Lithospheric stress and uppermantle dynamics in mainland China due to mantle flow based on combination of global- and regional-scale seismic tomography. *J. Asian Earth Sci.*, *132*, 103–117. https://doi.org/10.1016/j.jseaes.2016.10.004